ADVANCES IN GEODESY AND GEOINFORMATION
(formerly GEODESY AND CARTOGRAPHY)
Vol. 71, no. 1, article no. e19, 2022

https://doi.org/10.24425/gac.2022.141172

Original paper

Part of Topical collection:
"Advancements in Applied Geoinformatics"

On the applicability of integrated UAV photogrammetry and automatic feature extraction for cadastral mapping

Oluibukun Gbenga Ajayi, Emmanuel Oruma

Federal University of Technology, Minna, Nigeria
e-mail: ogbajayi@gmail.com; ORCID: http://orcid.org/0000-0002-9467-3569
e-mail: orumaemmy2020@gmail.com; ORCID: http://orcid.org/0000-0002-8203-484X

*Corresponding author: Oluibukun Gbenga Ajayi, e-mail: ogbajayi@gmail.com

Received: 2021-02-18 / Accepted: 2022-04-04

Abstract: The applicability of integrated Unmanned Aerial Vehicle (UAV)-photogrammetry and automatic feature extraction for cadastral or property mapping was investigated in this research paper. Multi-resolution segmentation (MRS) algorithm was implemented on UAV-generated orthomosaic for mapping and the findings were compared with the result obtained from conventional ground survey technique using Hi-Target Differential Global Positioning System (DGPS) receivers. The overlapping image pairs acquired with the aid of a DJI Mavic air quadcopter were processed into an orthomosaic using Agisoft metashape software while MRS algorithm was implemented for the automatic extraction of visible land boundaries and building footprints at different Scale Parameter (SPs) in eCognition developer software. The obtained result shows that the performance of MRS improves with an increase in SP, with optimal results obtained when the SP was set at 1000 (with completeness, correctness, and overall accuracy of 92%, 95%, and 88%, respectively) for the extraction of the building footprints. Apart from the conducted cost and time analysis which shows that the integrated approach is 2.5 times faster and 9 times cheaper than the conventional DGPS approach, the automatically extracted boundaries and area of land parcels were also compared with the survey plans produced using the ground survey approach (DGPS) and the result shows that about 99% of the automatically extracted spatial information of the properties fall within the range of acceptable accuracy. The obtained results proved that the integration of UAV-photogrammetry and automatic feature extraction is applicable in cadastral mapping and that it offers significant advantages in terms of project time and cost.

Keywords: land management, remote sensing applications, image segmentation, automatic boundary extraction, UAV mapping

1. Introduction

Unmanned Aerial Vehicles (UAVs), popularly known as drones, are aerial vehicles or aircrafts controlled remotely by a human operator or autonomously by an onboard computer (http://nesac.gov.in/uav-applications/). It uses a combination of Global Positioning System (GPS) navigation technology and aircraft model technology to provide fast and affordable mapping services (Barnes et al., 2014). These autonomously flying systems are typically equipped with a variety of navigation, positioning and mapping sensors, such as still video cameras, and others (Manyoky et al., 2011). Global Navigation Satellite System (GNSS) enabled UAVs have prospective application for quicker, accurate, and less costly remote data collection than piloted aerial vehicles (Ajayi et al., 2018).

The growing use of UAVs for photogrammetric mapping in aerial surveys is unprecedented. Due to the fact that UAVs are relatively cheap, and the increasing global need for access to information on land-based properties as a basis for resource planning, growth and control (Barnes et al., 2014), the utilization of UAVs in land administration and cadastral mapping is fast gaining acceptable attention and critical investigation. Using UAVs in mapping custom lands, urban lands, etc., cadastral maps of high resolution can be easily produced within a short time. The system is fast and easy to use, and it produces comprehensible plot representations as opposed to polygons with no graphic background. The high-resolution orthomosaics generated from the UAV-acquired 2D overlapping images allow the user to identify features that guide property identification and mapping. Such features include footpaths, fields of crops, building footprints like walls, edges, or any identifiable features.

It is very important to update information about land boundaries so that changes in ownership and property division can be documented on time. One of the benefits of using aerial imageries is that they provide a historical record of the places that may be revisited to see what changes have occurred in the future. Archived images can thus provide useful evidence where there are conflicts in the boundary of parcels. In contrast, classical approaches to land and property surveying are time-consuming and require a great deal of effort. In remote areas, particularly in mountainous areas, and when the weather is harsh, it is sometimes very difficult to carry out such surveys. In this situation, aerial photographs can be used as an alternative to classical survey method for the acquisition of spatial information where most measurements can be performed in the office or remotely (Eisenbeiss, 2009). UAV is now employed as a data acquisition platform for the extraction of spatial information of land-based properties (creation and update of cadastral maps) due to its rapid development over the past few years though predominantly through manual delineation of visible cadastral boundaries (Karabin et al., 2021).

Rijsdijk et al. (2013) investigated the usefulness of UAVs in the juridical verification process of cadastral borders of ownership at Het Kadaster; the national land registration service and mapping agency in the Netherlands, using AscTec Falcon 8, Microdrone MD-4 drones. Also, Crommelinck et al. (2016) and Karabin et al. (2021) presented an overview of different case studies investigating the applicability and potentials of UAVs for cadastral mapping and boundary delineation. However, most of the documented case

studies deal with manual boundary delineation, with very little attempts to proffer solution to the problem of automatic delineation of cadastral boundaries which is recently gaining wide attention with the advent of machine learning and computer vision. Since a large number of property boundaries are assumed to be visible, as they coincide with natural or manmade object or features such as building footprints (Zevenbergen and Bennett, 2015; Crommelinck et al., 2017), this makes them potentially extractable automatically (Jazayeri et al., 2014) using computer vision methods and algorithms that detect object contours in images.

The aim of this research is to investigate the applicability and efficiency of implementing multi-resolution segmentation (MRS); an object-based approach, at different scale parameters (SP), for the automatic extraction of visible cadastral boundaries (depicted by building footprints) from UAV images.

1.1. Imagery-Based Boundary Detection – review

In recent years, research efforts have shown how image-based cadastral mapping is being explored to acquire and modify data quickly and cost-effectively. Manual digitization for image-based boundary detection and delineation has been performed in early practices (Manyoky et al., 2011; Ali and Ahmed, 2013; Parida et al., 2014) and the results affirmed that more landed properties can be mapped in less time using high-resolution imagery. Research has also recently shown that image processing and computer vision offer new opportunities to replace manual approaches with an automated approach. Babawuro and Beiji (2012) detected field boundaries from satellite images using canny edge detection and morphological activities by connecting the segmented boundaries with Hough transformation. Though some boundaries were not accurately captured by the method, the findings of the research showed that the implementation of machine vision and integrating it with cadastral mapping, brings about substantial benefits like reduction in personnel and human efforts. Nyandwi (2018) used object-based image analysis (OBIA) to extract cadastral parcels using multi-resolution segmentation and chessboard approach. An object-based approach refers to the extraction of object outlines based on a cluster of pixels with similar characteristics and is applied to high-level features which represent shapes in an image (Crommelinck et al., 2016). The approach was tested using pan-sharpened Worldview-2 imagery at an urban site and a rural site in Rwanda. For precision measurement, reference lines were given a tolerance of 5 m. The method obtained an accuracy of 47.4% and completeness of 45% in rural areas. The authors argued that the findings were counterintuitive in urban areas and that the recovery of residential parcels is difficult for machine vision because the spectral reflection of the roof, garden, and fences in this area varies significantly.

Puniach et al. (2018) posited that an orthomosaic and digital surface model (DSM) generated from UAV-acquired images can be used for updating and maintaining a cadaster. The findings of their research further affirmed that UAV approach can produce significantly better results when multiple ground control points (GCPs) are used, compared to the result obtained from GNSS survey in Real Time Kinematic (RTK) mode.

Also, Wassie et al. (2018) implemented a mean-shift segmentation algorithm; a QGIS open source plugin used for segmentation of objects, to delineate cadastral boundaries. Using Worldview-2 images with a resolution of 0.5 m, three rural areas in the Amhara State of Ethiopia, were used as the test sites for the investigation. The buffer widths from the reference boundary were 0.5 m, 1 m and 2 m, and the obtained results showed 16.3%, 24.7% and 34.3% overall accuracy for the first (SI1) selected area. The extractions with mean-shift segmentation are closed object boundaries in vector format and were found to be topologically correct. The mean-shift segmentation was applied to a full extent of satellite images while some of the automatic object extraction methods were applied also using UAV images (Fetai et al., 2019). They also affirmed that almost 80% of the extracted visible boundaries were adjudged to be correct when buffer overlay technique was applied, which shows the potential of cadastral mapping based on UAV imagery.

Furthermore, Luo et al. (2017) investigated cadastral boundaries extraction in urban areas from airborne laser scanner data, designing a semi-automatic workflow with post-refining and automatic extraction of features. Objects such as buildings and roads were segmented in the automatic extraction process using canny edge detector, alpha shape, and skeleton algorithms, while objects such as fences were delineated using centerline fitting techniques. Since not all artefacts extracted were cadastral boundaries, the post-refinement process involves manual support. Visual interpretation in this phase was adopted for the extraction of useful line segments and gaps between line segments were filled manually. With a tolerance of 4 m from the reference boundaries, the designed workflow achieved completeness of 80% and correctness of 60%.

In addition, Crommelinck et al. (2017) studied the transferability of globalized probability of boundary (gPb) contour detection technique to UAV images for the automatic detection and extraction of contours for UAV-based cadastral mapping. The result of their investigation using three UAV orthoimages of different extents showing rural areas in Germany, France and Indonesia, shows that the approach is transferable to UAV data and automated cadastral mapping by obtaining completeness and correctness rates of up to 80%.

In order to speed up the process of establishing, maintaining and updating cadastres, Fetai et al. (2019) investigated the potentials of high-resolution optical sensors on UAV platforms for cadastral mapping, using the feature extraction (FX) module of ENVI for data processing. The findings of the study show that about 80% of the extracted boundaries were adjudged correct, while emphasizing on the importance of filtering the extracted boundary maps for the improvement of the results. The described image processing workflow shows that the approach is mostly applicable when the UAV orthoimage is resampled to a larger ground sample distance (GSD). In addition, the findings show that it is important to filter the extracted boundary maps to improve the results.

Also, Crommelinck et al. (2020) developed a methodology that automatically extracts and processes candidate cadastral boundary features from UAV data, consisting of two state-of-the-art computer vision methods, namely gPb contour detection and simple linear iterative clustering (SLIC) super pixels, as well as a classification part assigning costs to each outline according to local boundary knowledge. The developed methodology also

included a procedure for a subsequent interactive delineation; a user-guided delineation by calculating least-cost paths along previously extracted and weighted lines. The approach was tested on visible road outlines in two UAV datasets obtained from two rural areas in Amtsvenn and Gerleve (Germany), processed using Pix4Dmapper, and the obtained results show that all roads can be delineated comprehensively. When the developed automatic approach was compared to manual delineation, the number of clicks per 100 m reduced by up to 86%, while obtaining a similar localization quality.

Fetai et al. (2020) investigated the applicability of U-Net architecture; a symmetric network containing two parts which gives it a U-shaped architecture, for the automatic detection of visible boundaries from UAV images captured with the aid of a DJI Phantom 4 drone. The architecture was designed using Python and implemented in high-level neural network API Keras (François et al., 2015) running within TensorFlow library, while the training of the BSDS500 datasets (which were concatenated to increase the flexibility in the validation split and the number of training samples) was done through Google Colaboratory which provided a stronger GPU, more memory, and efficient calculations, with the evaluation metrics of the trained model indicating 0.95 overall accuracy. While the average %age of correctly detected visible boundaries was estimated to be almost 80% for the tiled UAV images, the study found out that the automatic boundary detection using U-Net is applicable mostly for rural areas where the visibility of the boundaries is continuous (Luo et al., 2017). The model was evaluated by monitoring the loss and accuracy of training, and validation data using binary cross-entropy was used as a loss function while overall accuracy was adopted as the evaluation metric.

Using Pléiades images, the performance of random forest (RF) when compared with other classifiers such as the support vector machines (SVM), maximum likelihood, and the back propagation neural networks in the automatic extraction of building lines or footprints was investigated by Taha and Ibrahim (2021). Results of the assessment showed that the RF, SVM, maximum likelihood, and back propagation yielded an overall accuracy of 97%, 93%, 95% and 92%, respectively, which proved that the RF outperformed the other classifiers. Also, the completeness and correctness of the extracted footprints using RF indicated that it can accurately classify 100% of buildings.

While different algorithms have been implemented for automatic boundary delineation or property line extraction, most of such experiments have been conducted on satellite or other remotely sensed images while there is relatively sparse evidence of past documented efforts aimed at implementing object oriented automatic feature extraction algorithms on UAV acquired images for property or cadastral mapping as presented in this research.

1.1.1. Edge Detection Techniques

Edge detection is one of the most important features in the application of machine vision, computer vision, image processing and analysis (Zhang et al., 2013; Selvakumar and Hariganesh, 2016). The goal of edge detection is to extract information from object

boundaries within the image by detecting discontinuities or abrupt changes in brightness level. Edges provide the image's boundaries between different regions. The boundaries obtained are useful for the recognition of objects within image for segmentation and for matching purposes (Chai et al., 2012). Edge detection has also attracted enormous attention in medical imaging such as MRI (Giuliani, 2012; Aslam et al., 2015), ultrasound (Chai et al., 2012), CT (Punarselvam and Suresh, 2011; Bandyopadyay, 2012) and X-ray images (Lakhani et al., 2016), road mapping analysis (Sirmacek and Unsalan, 2010; Qui et al., 2016), and other applications, even with the enhancement of noisy satellite images (Jena et al., 2015; Gupta, 2016).

Image segmentation and edge detection are the predominantly used algorithms for semi-automatic or automatic boundary delineation (Crommelinck et al., 2016). Segmentation refers to partitioning images into disjointed regions, where the spectral characteristics of the pixels are similar to each other (Pal and Pal, 1993). On the other hand, edge detection algorithms detect edges in brightness and colour as sharp discontinuities (Bowyer et al., 2001).

Object oriented image analysis has become an important issue in the field of image processing and interpretation. The basic idea behind this approach is to segment an image into parcels, extract features from the segmented parcels, and then complete the image interpretation by classifying its features. The major advantage of object-oriented image analysis is that it deals with parcels, not pixels. These parcels are objects, which provide abundant features and spatial knowledge involved in analysis (Aplin et al. 1999). Object-based image analysis methods are based on aggregating similar pixels to obtain homogenous objects, which are assigned to a target class.

The basic concept of creating an image object is to merge adjacent pixels where the heterogeneity is minimized, and while maintaining its acceptability to human vision. Recently, the implementation of MRS algorithm is gaining wide attention for different applications. Munyati (2018) implemented MRS for the delineation of savannah vegetation boundaries. The result of the studies showed that an overall mapping accuracy of 86.2% was obtained. He also posited that the successful delineation of the savannah vegetation communities indicated that pre-segmentation and analysis of potential objects variance-based texture can provide guidance on parameter values to be specified for the inherently iterative MRS. Chen et al., (2019) developed an approach for MRS parameter optimization and evaluation for very high resolution (VHR) remote sensing images based on mean nanoscience and quantum information (meanNSQI). The findings of the experimentation showed that a discrepancy measure of 85% accuracy was obtained which proved that the segmentation parameter optimization and quality evaluation given by meanNSQI and the discrepancy measure are reliable.

Furthermore, Kohli et al. (2017) investigated the applicability of MRS and estimation of scale parameter (ESP); an object-based approach for the extraction of visible cadastral boundaries from high resolution satellite images (HRSI). Pixel-based accuracy assessment method was adopted and the quality of the feature detection and extraction in terms of error of commission and omission were 75% and 38%, respectively, for the MRS, and 66% and 58%, respectively for the ESP. Within a 41–200 cm distance from

the reference boundaries, the localization quality of 71% and 73% was obtained for the MRS and ESP, respectively. The result showed that it is difficult to achieve a balance between high %age of completeness and correctness, and concluded that the resulting segments can potentially serve as a base for further aggregation into tenure polygons using participatory mapping.

1.2. Multi-resolution segmentation

MRS is an area-fusing or region based image segmentation algorithm (Witharana and Civco, 2014) that begins with each pixel forming an entity or region (Baatz and Schape, 2000). It is often used as a general segmentation algorithm in the field of remote sensing applications (Neubert et al., 2007) because of its ability to generate image objects with greater geographical significance and strong adaptability (Martha et al., 2011).

The merging criterion for MRS is local homogeneity, which describes the similarity between adjacent objects. The fusion process stops when all potential fusions meet the requirements for homogeneity. MRS relies on several parameters, which are image layer weights, scale parameter (SP), shape and compactness. Image layer weights define the importance of each image layer to segmentation process. For the experiment reported in this paper, equal weights have been apportioned to the three layers; Red, Green and Blue (RGB) of the input image to ensure a more regular shape of the merged parcel because apportioning different weights to the image layers will cause unfair segmentation which will affect the regularity of the shape. The most important parameter in MRS is the scale, which controls the average image object size (Draguţ et al., 2014). A larger SP allows higher spectral heterogeneity within the image objects, hence allowing more pixels within one object. Defining the appropriate SP is very critical for the successful implementation of MRS algorithm and attempt has been made in this research to explore the effect of different SPs in the automatic extraction of visible cadastral boundaries and building footprints with a view to identifying appropriate SP for automatic feature extraction in cadastral mapping using MRS algorithm.

1.2.1. Merging Criterion

A merge cost function that integrates spectral and shape heterogeneity is designed to guide the merging of parcels. The use of shape is to make the outline of the merged parcels more regular. Experimentally, the merging cost function is similar to Eq. (1) according to Baatz and Schäpe, 2000):

$$f = w \times h_{\text{color}} + (1 - w) \times h_{\text{shape}} \tag{1}$$

where w is the weight dropping in the interval $[0,\ 1]$ for spectral heterogeneity. A typically acceptable color weight is 0.9 and form weight is 0.1. This causes unfair segmentation when the form weight is too large.

The spectral heterogeneity is the parent parcel variance less the sum of the variances of the two children's parcels weighted with their respective areas:

$$h_{\text{color}} = \sum_{c} w_c \left(n_{\text{merge}} \sigma_c^{\text{Merge}} - \left(n_1 \sigma_c^1 + n_2 \sigma_c^2 \right) \right) \tag{2}$$

where c is the band count and w_c is user specified weights for every band (1.0 by default).

The shape heterogeneity (Eq. (3)) is the combination of compactness and smoothness heterogeneity, in which compactness heterogeneity is calculated using Eq. (4) and smoothness heterogeneity is calculated using Eq. (5):

$$h_{\text{shape}} = w_{\text{cmpct}} \times h_{\text{cmpct}} + (1 - w_{\text{cmpct}}) \times h_{\text{smooth}} \tag{3}$$

$$h_{cmpct} = n_{\text{Merge}} \cdot \frac{l_{\text{Merge}}}{\sqrt{n_{\text{Merge}}}} - \left(n_1 \cdot \frac{l_1}{\sqrt{n_1}} + n_2 \cdot \frac{l_2}{\sqrt{n_2}} \right) \tag{4}$$

$$h_{\text{smooth}} = n_{\text{Merge}} \cdot \frac{l_{\text{Merge}}}{b_{\text{Merge}}} - \left(n_1 \cdot \frac{l_1}{b_1} + n_2 \cdot \frac{l_2}{b_2} \right) \tag{5}$$

where l is the perimeter of a parcel, n is the pixels, b is the perimeter of its bounding box. A commonly suitable setting of w_{cmpct} is 0.5.

2. Materials and methods

2.1. Study area

The study area selected for this study is popularly known as Kuje Low-Cost, a residential estate located in Kuje Area Council in the Nigeria's Federal Capital Territory (FCT), Abuja. The mapped area has a total area of 224 000 square meters (22.4 hectares). It lies within the boundary of Northings 982 870.00 mN to 982 300.00 mN and Eastings 306 000.00 mE to 306 700.00 mE. The principal characteristics that informed the choice of this study area are the configuration of the area's terrain which is neither too rough nor too gentle, and also, the area is a planned urbanized zone with land parcels delineated by visible linear features and clear building footprints. Figure 1 depicts the map of the study area.

2.2. Data acquisition and processing

Site reconnaissance was first conducted to identify suitable locations for the establishment of ground control points (GCPs), and check points (CPs) in the study area. During this process, the points or stations identified for the GCPs and CPs were pre-marked. Dronedeploy; a flight planning software was used to design the flight plan which was used for the image data acquisition.

GCPs are very important for georeferencing the images and for qualitative analysis of the positional data. Stations pre-marked for the establishment of GCPs were properly

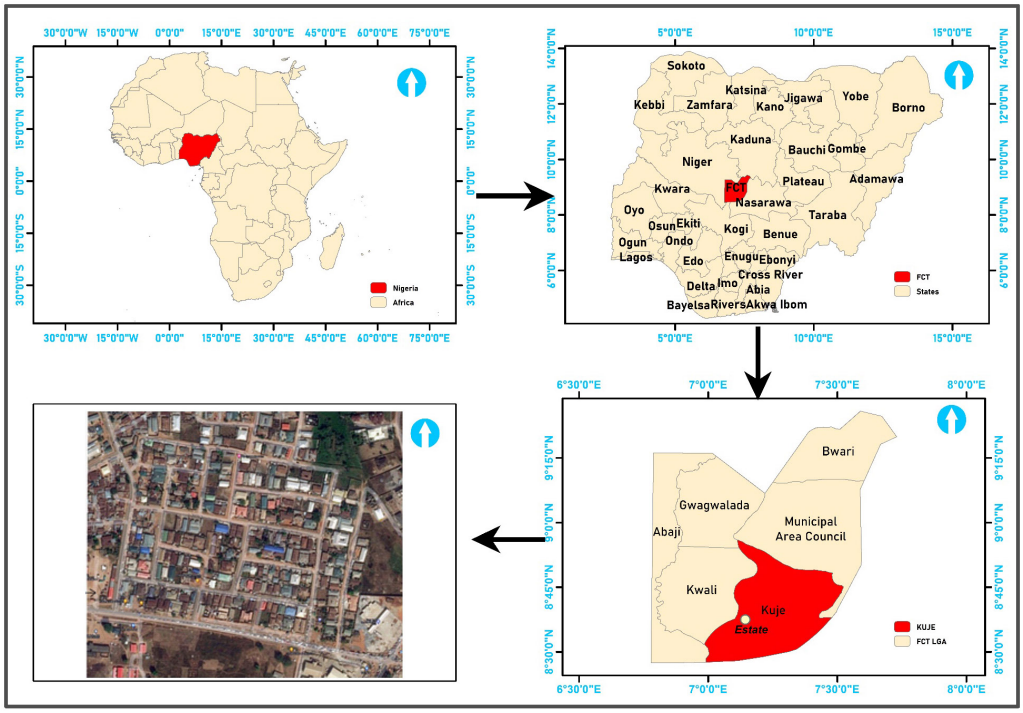

Fig. 1. Map of the study area

fixed and established using Hi-Target DGPS receivers to acquire their positional data. A total of Eight (8) ground stations were established within the study area, out of which Five (5) were used as the CPs while the remaining three (3) were used as GCPs. Markers were used to mark the points defining the established stations, a sample of which is shown in Figure 2b. For the GNSS data acquisition, two units of Hi-Target DGPS receivers, with one serving as a base (mounted on the base station) while the other served as rover (roving through the pre-marked ground stations), were used to acquire positional data of the control stations with the rover spending a minimum of 20 minutes of occupation time on each of the stations. The point datasets (coordinates) recorded on the Hi-Target DGPS receivers were imported into Carlson with AutoCAD 2012 for further processing and plotting. Table 1 presents the details of the date and time of observation, standard deviation of the coordinates (Nrms, Erms and Zrms), and the position dilution of precision (PDOP) values which describe the error caused by the relative position of the GPS satellites obtained for each of the established ground control stations. The elevation mask value was 5 and it was uniformly applicable to all the control points while a uniform antenna height of 1.881 m was adopted for the measurements.

Also, a total of 785 overlapping images were captured at 70 m flying height, using DJI Mavic Air UAV on-board camera with an integrated 12 megapixels CMOS sensor and f/2.8 lens, and with a 35 mm equivalent focal length of 24 mm to shoot high-quality photos and videos.

Table 1. Details of the GNSS observation

Name	N (m)	E (m)	Z (m)	Nrms (m)	Erms (m)	Zrms (m)	Start date and time	End date and time	PDOP	Sharing Sat Num
CP001	981911.090	306084.450	313.442	0.005	0.006	0.010	6/27/19 10:09	6/27/19 10:29	1.3	16
CP002	981896.420	306229.280	314.999	0.005	0.006	0.010	6/27/19 10:57	6/27/19 11:17	1.9	11
CP003	981871.980	306374.400	313.940	0.005	0.006	0.009	6/27/19 11:27	6/27/19 11:47	1.3	16
CP004	982002.170	306389.870	309.929	0.005	0.006	0.010	6/27/19 12:18	6/27/19 12:38	1.7	13
CP005	982116.230	306422.570	303.702	0.006	0.007	0.012	6/27/19 12:52	6/27/19 13:12	1.9	11
CP006	982022.600	306260.250	311.653	0.007	0.008	0.016	6/27/19 13:31	6/27/19 13:51	1.3	16
CP007	982150.160	306264.810	309.656	0.010	0.010	0.021	6/27/19 14:22	6/27/19 14:42	2.2	10
CP008	982041.910	306106.610	314.381	0.006	0.008	0.012	6/27/19 15:04	6/27/19 15:24	1.9	10

All acquired images were processed using Agisoft metashape digital photogrammetric software. The workflow for the processing includes the following; importation of photos into the software working environment, alignment of the imported photos, importation of GCPs, camera calibration, generation of dense point cloud, generation of Digital Surface Model (DSM), and generation of orthomosaic. The ground sampling distance of the generated orthomosaic is 1.44 cm/pix.

The orthomosaic generated from the photogrammetric software was imported into ArcMap 10.5 and eCognition Developer software for further processing and analysis, which includes the digitization of the land boundaries on the orthomosaic in order to aid the positional data comparison, and the implementation of the MRS algorithm.

2.3. Automation process

MRS algorithm was implemented in eCognition software (version 9) for the automatic extraction of the visible land boundaries. MRS is a region-merging technique starting from each pixel forming one image object or region (Baatz and Schäpe, 2000), which implies that improperly defined parcel boundary lines are difficult to automatically extract using this algorithm. This difficulty can however be overcome if the parcel boundary is defined by visible linear features such as fence lines or building footprints that are not covered with shades or canopies, though the technique gives better result for building lines and the results are influenced by the choice of SPs. SP is the most important parameter in the implementation of this algorithm because it controls the average image object size

(Draguţ et al., 2014). It is a subjective measure that controls the degree of heterogeneity within an image-object (Draguţ et al., 2010). Each SP can be generated independently based on the pixel level, or within a hierarchy, where a parent-child relationship exists between the levels. For this study, the ESP; a tool that builds on the idea of local variance (LV) of object heterogeneity within a scene was used for the scale parameter estimation within the eCognition image processing software (Draguţ et al., 2010; Kohli et al., 2018).

Since the key control for MRS algorithm is the SP, five (5) different SPs were experimented in order to obtain the optimal SP for the automatic extraction of parcels. The SP values were set at 150, 400, 500, 700, 1000 for the 5 different experiments with constant or fixed shape, and compactness values of 1.5 m and 0.8 m, respectively.

2.4. Accuracy assessment

For the orthomosaic accuracy assessment, positional data (coordinates) of the CPs were extracted from the produced orthomosaic. The Easting, Northing and Height (XYZ) component of the coordinates were compared with the GNSS acquired coordinates of the same CPs. The difference between the GNSS acquired coordinates and the extracted coordinates from UAV produced orthomosaic was estimated and used for the computation of change in planimetric coordinates using equation (5) which is the Euler's distance formula.

$$\Delta d = \sqrt{(x - x_1)^2 + (y - y_1)^2} \tag{6}$$

where Δd is the change in distance in meters, (x, y and x_1, y_1) are the coordinate of the two stations.

Also, the coordinates of the CPs were extracted for comparison with coordinates extracted from digitized orthomosaic and the discrepancy was computed using the Root Mean Square Error (RMSE) formula in Eq. (7).

$$\mathrm{RMSE} = \sqrt{\frac{\sum_{i=1}^{n} \left(y_{\mathrm{pred}} - y_{\mathrm{ref}}\right)^2}{n}} \tag{7}$$

where y_{pred} is the predicted value, y_{ref} is the reference value, and n is the total number of points.

2.4.1. Accuracy assessment of the automatic feature extraction

Since the output of the automatically extracted features is in vector format, the adopted strategy for the accuracy assessment was an object-based approach using buffer overlay method, which was also the method adopted by Fetai et al. (2019). The object-based approach consists of a matching procedure which is in two folds (Heipke et al., 1997); firstly, it yields those parts of the extracted data which are supposed to be boundaries,

road, building footprints, etc, and which corresponds to the reference data, and secondly, it shows which part of the reference data that indeed corresponds to the extracted data.

In the first step, both networks (extracted and reference data) are split into short pieces of equal length, after which a buffer of constant predefined width (buffer width = 150 cm) was constructed around the reference property data. The percentage of the reference data which is found within the buffer around the extracted data is referred to as completeness and its optimum value is 1 (i.e. 100%). According to the notation of McGlone and Shufelt (1994) and CMU (1997), the matched extracted data is denoted as *true positive* with length (TP), affirming that the extraction algorithm has indeed found a property data. The unmatched extracted data is denoted as *false positive* with length (FP), because the extracted property line hypotheses is incorrect, while the unmatched reference data is denoted as false negative (FN).

In the second step, matching is performed the other way round. The buffer is now constructed around the extracted property data, and the parts of the reference data lying within the buffer are considered to be matched. The percentage of the extracted property data which lies within the buffer around the reference network is known as correctness, and it represents the percentage of correctly extracted property data. Its optimum value is also 1 (Heipke et al., 1997).

In order to assess the accuracy of the automatically extracted features using the MRS algorithm, the completeness and correctness of the extraction at each of the experimented different SPs were computed using equations (8a) and (8b) and (9a) and (9b) respectively, while the overall accuracy (quality) was estimated using the expression in equation (10):

$$\text{Completeness} = \frac{\text{Length of matched reference}}{\text{Length of reference}} * 100\% \tag{8a}$$

$$C_p \approx \frac{TP}{TP + FN} * 100\% \tag{8b}$$

Also,

$$\text{Correctness} = \frac{\text{Length of matched extraction}}{\text{Length of extraction}} * 100\% \tag{9a}$$

$$C_r \approx \frac{TP}{TP + FP} * 100\% \tag{9b}$$

$$OA = \frac{\text{Length of matched extraction}}{\text{Length of extracted data} + \text{Length of unmatched reference}} * 100\% \tag{10}$$

where TP is the true positives, FP is the false positives, FN is the false negative (Galarreta et al., 2015), while C_p is Completeness, C_r is Correctness for low redundancy. OA is the overall accuracy which describes the "goodness" of the extraction. The overall accuracy which is also referred to as the measure of quality, takes into account the completeness of the extracted data as well as its correctness (Heipke et al., 1997).

2.5. Estimation of project execution time and cost

In order to estimate the project execution time for the two methods, the entire project was subdivided into different project components and the time expended for each of the component was recorded. Also, the expended cost of each of the project components was estimated by direct costing. While the approximate project time was documented in number of days, the project cost was estimated in Nigerian Naira (₦). As at the time of executing this research project (December, 2019), a US Dollar is exchanged to naira (₦) at an average rate of 362.61 naira to 1 USD on a concrete day. This was also around the same time the minimum monthly wage of Nigerian workers was increased from ₦18 000 to ₦30 000 by the Nigerian government.

3. Results and discussion

Figure 2a presents the orthomosaic generated from the acquired images which serves as the base map for the extraction of land boundaries, building footprints and other features while Figure 2b is a screenshot of a zoomed portion of the image showing a sample of the markers used for the GCPs. The land plots and building lines from the orthomosaic were obtained by two different techniques; which are manual digitization and automated feature extraction technique using MRS, while the ground survey parcel data was used as reference. Also, the manually digitized property boundary features were used as reference information for the automatically extracted features. Figure 3 depicts the AutoCAD drawing obtained from ground survey approach which was used as reference data for the UAV survey data.

(a) (b)

Fig. 2. (a) UAV orthoimage of the study area, (b) photo of the marker used for the GCP

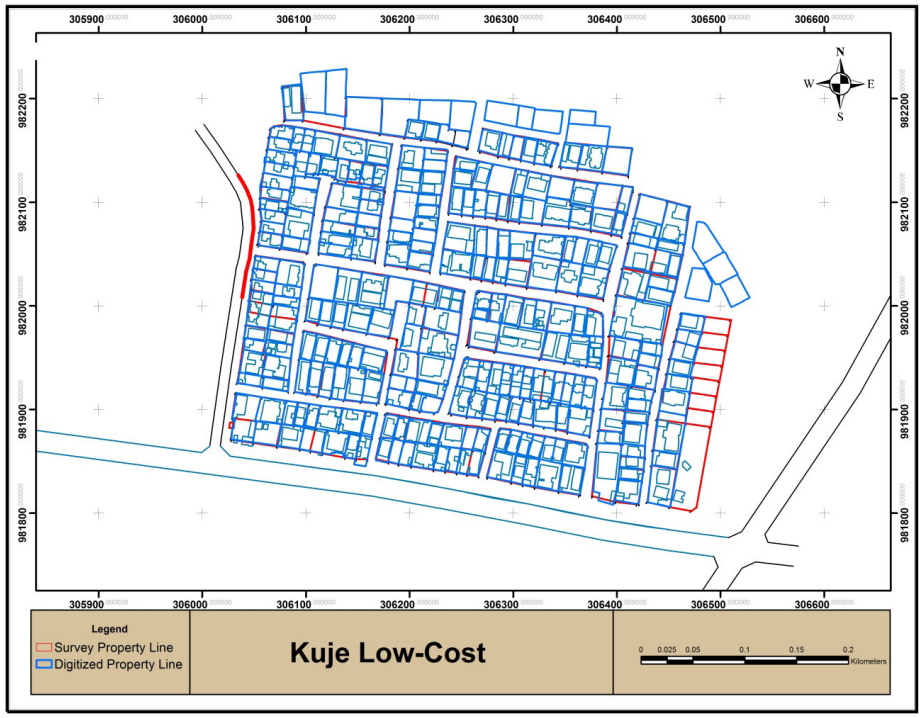

Fig. 3. Manually delineated visible cadastral boundaries surveyed with GNSS receiver, used as reference data

Other results obtained are the result of the accuracy evaluation of the automatically extracted visible boundaries using the MRS algorithm at different SPs (see Table 3 and Table 4), and the result of the cost and time comparison of the UAV and GNSS survey (see Table 5 and Table 6).

3.1. Scale Parameters of MRS

The results obtained when the SP of the MRS was set at 150, 400 and 500 are shown in Figure 4a–Figure 4c with the blue line depicting the boundary lines of every segment. It was observed that the output polygon continues to decrease with an increase in the value of the SP. Likewise, the visual clarity of the output polygon improves with increase in the value of the SP. When compared to the output of the automatically extracted visible boundaries using MRS with SP values 150 and 400 (Fig. 4a and Fig. 4b), the pixel level in the output map was observed to be decreasing continuously with increase in SPs as observed in the result obtained when the SP value was set at 500 (Fig. 4c).

Figure 5 presents the automatically extracted visible boundaries when the SP value of the MRS was set at 700, while Figure 6 presents the segmentation result obtained when the SP was fixed at 1000. Analysis of these two results showed that the pixel

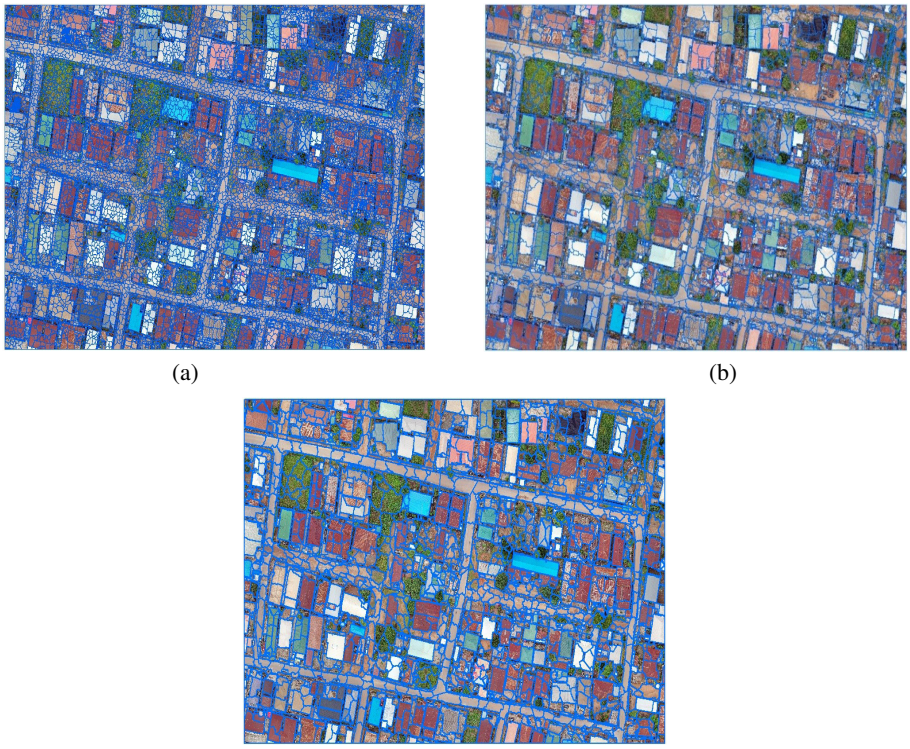

(a) (b)

(c)

Fig. 4. Automatically extracted visible boundary lines overlaid on the ground truth data. (a) at SP = 150, (b) at SP = 400, (c) at SP = 500

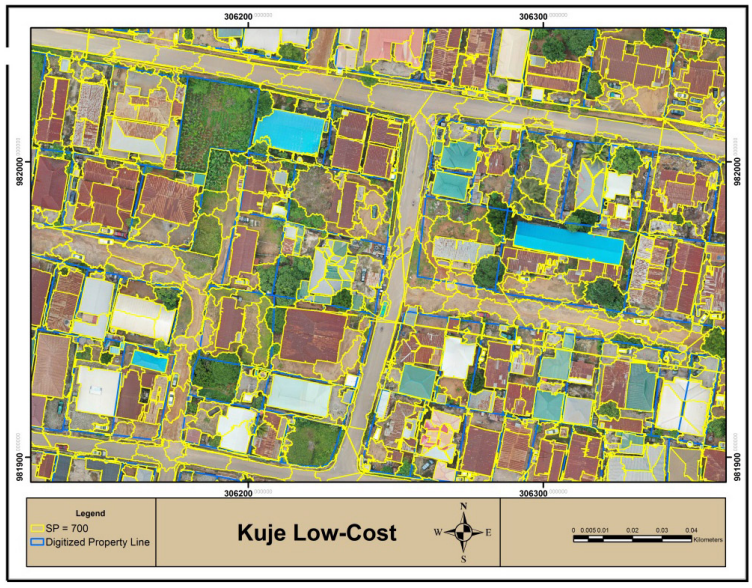

Fig. 5. Automatically extracted visible boundary lines overlaid on the ground truth data with SP = 700

level decreased with increased value of SP. The output map of SP = 1000 gives a more cartographically appealing result based on its stronger pixel level. The yellow line in Figure 5 shows the boundary lines of every segment when SP = 700 was used while the red line in Figure 6 shows the boundary lines of every segment when SP = 1000 was used.

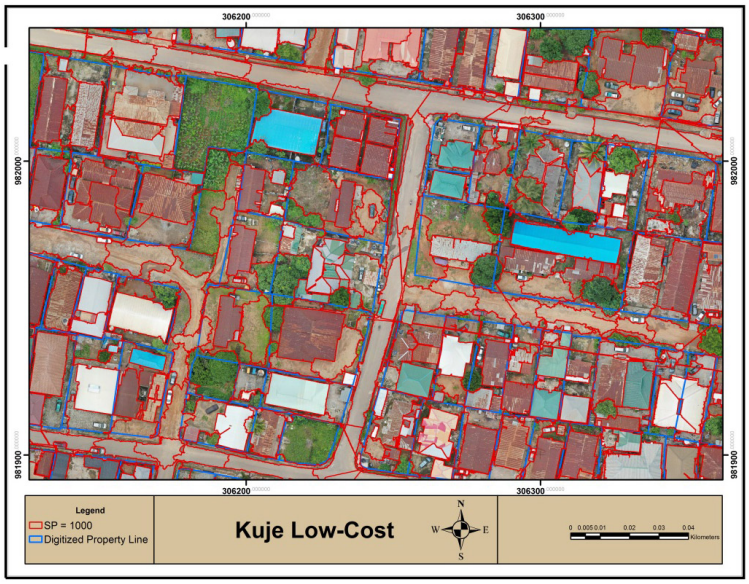

Fig. 6. Automatically extracted visible boundary lines overlaid on the ground truth data with SP = 1000

3.2. Accuracy assessment for the generated orthomosaic and automatic feature extraction

Table 2 presents the planimetric coordinates and discrepancy between the GNSS acquired coordinates and the extracted coordinates of the CPs from the UAV generated orthomosaic. From Table 2, ΔN (m) and ΔE (m) represents the difference in planimetric (northing and easting) coordinates as obtained from GNSS acquired data and UAV generated orthomosaic.

The obtained horizontal RMSE (RMSEx, y) as computed using equation (6) is 0.3575. This is consistent with the result obtained by Karabin et al. (2021) and it affirms the applicability of UAV in cadastral or property mapping.

The result of the estimated completeness, correctness and overall accuracy of the automatically extracted building footprints at different SPs is presented in Table 3, while the results obtained from the estimated completeness, correctness and overall accuracy of the automatically extracted land parcels at different SPs is presented in Table 4.

The result (see Table 3) shows that a completeness, correctness and overall accuracy of 16%, 12% and 14%, respectively, was obtained when the MRS algorithm was deployed

Table 2. Discrepancy between GNSS acquired coordinates and extracted coordinates

Control ID	Ground Survey		UAV Survey		Deviations		
	N (m)	E (m)	N (m)	E (m)	ΔN (m)	ΔE (m)	$\sqrt{(x-x_1)^2+(y-y_1)^2}$
CP001	981911.086	306084.448	981911.102	306084.420	−0.012	0.030	0.258
CP002	981896.422	306229.281	981896.467	306229.295	−0.047	−0.015	0.132
CP003	981871.979	306374.395	981872.011	306374.408	−0.031	−0.008	0.207
CP004	982002.171	306389.874	982002.185	306389.891	−0.015	−0.021	0.791
CP005	982116.230	306422.570	982116.216	306422.581	0.014	−0.011	0.329
CP006	982022.596	306260.252	982022.547	306260.251	0.053	−0.001	0.092
CP007	982150.160	306264.810	982150.129	306264.796	0.031	0.014	0.085
CP008	982041.911	306106.608	982041.943	306106.589	−0.033	0.021	0.379
						RMSEx, y =	0.3575

Table 3. Result of the MRS accuracy assessment of extracted building footprints

S/N	SP	Completeness (%)	Correctness (%)	Overall accuracy (%)
1	150	16	12	14
2	400	45	43	37
3	500	76	72	62
4	700	89	91	86
5	1000	92	95	88

Table 4. Result of the MRS accuracy assessment of extracted land parcels

S/N	SP	Completeness (%)	Correctness (%)	Overall accuracy (%)
1	150	25	19	18
2	400	38	32	22
3	500	43	37	25
4	700	52	48	32
5	1000	65	59	54

for the automatic extraction of the building lines or footprints at a SP = 150. When the SP was set at 700, 89% and 91% completeness and correctness, respectively were obtained with overall accuracy of 86% while an overall accuracy of 88% was obtained when the SP was set at 1000 with 92% and 95% completeness and correctness, respectively. Meanwhile, a completeness, correctness and overall accuracy of 25%, 18% and 19% was obtained when the SP was prefixed at 150 for the automatic extraction of land parcels (see

Table 4), while 65%, 59% and 54% were obtained for the completeness, correctness and overall accuracy, respectively, when the SP was set at 1000 for the automatic extraction of the land parcels using the MRS algorithm. The poor completeness, correctness and overall accuracy obtained from the automatically extracted land parcels when compared to the result of the building footprints can be attributed to the presence of shadows, unclear delineation of the boundary lines of the land parcels in vegetated areas, and the presence of mixed pixels in the automatic extraction (Horkaew et al., 2015; Wassie, 2016). The findings show that increase in the SP of the MRS algorithm also leads to increase in the obtained completeness, correctness and overall accuracy for the extraction of the building footprints and the land parcels. Also, it was observed that optimal completeness, correctness and overall accuracy of the automatic feature extraction was obtained when the SP was set at 1000, while setting the SP at 150 will not yield a reliable result. The result of the accuracy assessment is consistent with the findings of Luo et al. (2017), Munyati (2018) and Chen et al. (2019).

3.3. Cost and time comparison

The results obtained from the time and cost analysis of the integrated UAV-photogrammetry approach and the GNSS survey methods used for the survey of 248 land parcels are presented in Table 5 and Table 6, respectively.

Table 5. Summary of the project components and the execution timeframe (number of days)

UAV Photogrammetry method						
Activities	Reconnaissance	GCPs and CPs	UAV flight mission	Image processing	Digitizing	Other duties
No of days	2	1	1	2	3	3
No of persons	3	2	3	2	1	2
Total No of Days = 12						
Total No of Persons = 13						
Classical (GNSS) method						
Activities	Reconnaissance	Data Acquisition	Data filtering, processing and plotting			Others
No of days	2	18	7			3
No of persons	3	6	4			3
Total No of Days = 30						
Total No of Persons = 16						

From the results presented in Table 5 and Table 6, it can be observed that the parcel boundary extracted using GNSS method requires more intense field observation, thus, it consumes more time and cost. However, cadastral boundary extractions from UAV generated orthomosaic involves less field work and more off-field processing, and it is also more economical when compared to the GNSS method. Based on the time analysis,

Table 6. Cost comparison between UAV mapping and classical GNSS survey approach

Activity	Number of days	Cost (N)
UAV survey		
Reconnaissance	2	80 000
GCP	1	70 000
UAV Flight mission	1	200 000
Image Processing	2	500 000
Digitizing	3	150 000
Other	3	190 000
Total	12	1 190 000
Number of land parcels surveyed		248
Estimated cost of survey per land parcel (N)		4 798
Ground survey		
Reconnaissance	2	140 000
Data Collection	18	10 620 000
Data filtering, processing and plotting	7	250 000
Others	3	150 000
Total	30	11 160 000
Number of land parcels surveyed		248
Estimated cost of survey per land parcel (N)		45 000

it was observed that the total time taken to map the 248 properties using the UAV photogrammetry approach was just about one-third (1/3) of the total time expended when GNSS method was adopted. While the project was executed within just 12 days using the UAV approach, it took a total of 30 days for the project to be completed using the conventional GNSS approach which shows that the integrated UAV approach is 2.5 times faster than the conventional GNSS approach, even when the same manpower was deployed for the project.

It was also observed that the cadastral boundary obtained using GNSS method requires more personnel, equipment and resources for detail field observation and data processing. However, less human effort with very few equipment is required for UAV data capturing and image processing, and also in vectorizing the UAV generated orthomosaic, which is also consistent with the findings of Karabin et al. (2021). The results obtained from the cost comparison of these two approaches as presented in Table 6 shows that a total amount of N1 190 000.00 was expended for the mapping of 248 land parcels at the cost of less than N5 000.00 per parcel when the UAV approach integrated with the automatic feature extraction was used, while an approximate cost of N11 160 000.00 was expended when GNSS approach was used to survey the same 248 land parcels at an average cost of N45 000.00 per parcel. This implies that for large scale property mapping, the presented

UAV approach integrated with automatic feature extraction is approximately nine (9) times cheaper or less expensive than the classical GNSS surveying approach without compromising the obtainable accuracy.

4. Conclusions

The principal objective of this research is to investigate the applicability of UAV photogrammetry integrated with automatic feature extraction for cadastral mapping. MRS algorithm with different SP was implemented for the automatic extraction of visible cadastral boundaries defined by linear features defined nodes and building footprints. The result obtained from the automatic feature extraction shows that the accuracy of the cadastral boundary line extraction depends majorly on the SP which is the key control of the MRS algorithm. For the experiments conducted using varying SPs and constant shape and compactness value, the result obtained shows that the pixel level in the output map decreases continuously with increase in SPs while the optimal result of the conducted experiment was obtained when the SP was set at 1000, while the shape and compactness values were set at 1.5 m and 0.8 m, respectively. The result of the evaluation of the reliability of the automatic extraction also shows that the completeness, correctness and overall accuracy or quality increases with increase in the value of the SPs. Also, the MRS algorithms proved to be more efficient in automatically extracting building footprints when compared to its performance in the extraction of land parcels.

Furthermore, the results of the accuracy assessment obtained from the integrated UAV approach when compared with conventional survey approach shows that 99% of automatically extracted property boundaries from the UAV survey falls within the minimum acceptable horizontal accuracy for cadastral and property mapping of third order (1:5,000). Further analysis on the cost and time expended for the property mapping using the integrated approach shows that the approach is approximately 2.5 times faster and 9 times cheaper than the conventional ground surveying approach, especially when GNSS receivers are used for the spatial data acquisition. While MRS algorithm has proved to be a veritable model for automatic extraction of building footprints in cadastral mapping in this study, further research efforts shall seek to investigate the applicability of other segmentation algorithms in the automatic extraction of land parcel boundaries for cadastral applications. Meanwhile, it should be noted that the automatic extraction of boundaries is only a step to the facilitation cadastral mapping, as mere detecting and extracting the boundaries alone is not sufficient for complete and correct cadastral mapping.

Author contributions

Conceptualization: O.G.A.; research concept and design: O.G.A.; article writing: O.G.A.; critical revision of the article and final approval of the article: O.G.A.; collection and assembly of data: O.E.; data analysis and interpretation: O.E.; writing of the article draft: O.E.

Data availability statement

The data that support the findings of this study are available from the corresponding author upon reasonable request.

Acknowledgements

The authors would like to thank the anonymous reviewers and the editor for their constructive comments and contributions.

References

Ajayi, O.G., Palmer, M., and Salubi, A.A. (2018). Modelling farmland topography for suitable site selection of dam construction using unmanned aerial vehicle (UAV) photogrammetry. *Remote Sens. Appl: Soc. Environ.*, 11, 220–230. DOI: 10.1016/j.rsase.2018.07.007.

Ali, Z., and Ahmed, S. (2013). Extracting parcel boundaries from satellite imagery for a Land Information System. In 6th International Conference on Recent Advances in Space Technologies (RAST), 12-14 June. pp. 79–81. Istanbul, Turkey.

Aplin P., Atkinson P., Curran P., (1999). Per-field classification of land use using the forthcoming very fine resolution satellite sensors: problems and potential solutions. In: Advances in Remote Sensing and GIS Analysis. Chichester: Wiley and Sons Inc., 219–239.

Aslam, A., Khan, E., and SufyanBeg, M.M. (2015). Improved edge detection algorithm for brain tumor segmentation. *Procedia-Procedia Computer Science*, 58, 430–437. DOI: 10.1016/J.PROCS.2015.08.057.

Baatz, M., and Schape, A. (2000). Multiresolution segmentation: an optimization approach for high quality multi-scale image segmentation. Retrieved February, 2022, from http://www.ecognition.com/sites/default/files/405baatzfp12.pdf.

Babawuro, U., and Beiji, Z. (2012). Satellite imagery cadastral features extractions using image processing algorithms: A variable option for cadastral sciences. *Int. J. Comput. Sci.*, 9(4), 30–34.

Bandyopadyay, S.K. (2012). Edge detection from CT images of lung. *Int. J. Eng. Sci. Adv. Tech.*, 2(1), 34–37.

Barnes, T., and Engel, A. (2014). The photogrammetric potential of low-cost UAVs in forestry and agriculture. International Archives of the Photogrammetry, Remote Sensing and Spatial Information Science, XXXVI pp. 16–19. Retrieved February, 2022, from http://www.isprs.org/proceedings/XXXVII/congress/1pdf/206.pdf.

Bowyer, K.K., Kranenburg, C., and Dougherty, S. (2001). Edge detector evaluation using empirical ROC curves. *Comput. Vis. Image Underst.*, 84(1), 77–103. DOI: 10.1109/CVPR.1999.786963.

Chai, H., Wee, L.K., and Supriyanto, E. (2012). Edge detection in ultrasound images using speckle reducing anisotropic diffusion in canny edge detector framework. WSEAS Trans. on Biology and Biomedicine, 8(2), 51–60. Retrieved February, 2022 from http://www.mendeley.com/research/edgedetection-ultrasound-images-using-speckle-reducing-anisotropicdiffusion-canny-edge-detector-fr/.

Chen, Y., Qiang, C. and Changfeng, J. (2019). Multi-resolution segmentation parameters optimization and evaluation for VHR remote sensing image based on meanNSQI and discrepancy measure. *J. Spat. Sci.*, 66(2), 253–278. DOI: 10.1080/14498596.2019.1615011.

CMU (1997). Performance evaluation for feature extraction. Slides presented at the Terrain Week 1997. Retrieved from February 2022, http://www.cs.cmu.edu/afs/cs/usr/maps/www/rcvw/terrainweek97/roads/tw97-roadeval.ROOT.html.

Crommelinck, S., Bennett, R., Gerke, M. et al. (2016). Review of automatic feature extraction from high-resolution optical sensor data for UAV-Based cadastral mapping. *Remote Sens.*, 8, 689. DOI: 10.3390/rs8080689.

Crommelinck, S., Bennett, R., Gerke, M. et al. (2017). Contour detection for UAV-based cadastral mapping. *Remote Sens.*, 9, 171. DOI: 10.3390/rs9020171.

Crommelinck, S., Höfle, B., Koeva, M.N. et al. (2020). Interactive cadastral boundary delineation from UAV data. *ISPRS Ann. Photogr. Remote Sens. Spat. Inf. Sci.*, IV-2, 81–88. DOI: 10.5194/isprs-annals-IV-2-81-2018.

Draguţ, L., Tiedec, D., and Levick, S.R. (2010). ESP: a tool to estimate scale parameter for multiresolution image segmentation of remotely sensed data. *Int. J. Geogr. Inf. Sci.*, 24(6), 859–871. DOI: 10.1080/13658810903174803.

Draguţ, L., Csillik, O., Eisank, C. et al. (2014). Automated parameterization for multi -scale image segmentation on multiple layers. *J. Photogr. Remote Sens.*, 88, 119–127. DOI: 10.1016/j.isprsjprs.2013.11.018.

Eisenbeiss, H. (2009). UAV Photogrammetry. Retrieved from February 2022, http://www.igpdata.ethz.ch/berichte/blaue_berichte_pdf/105.pdf.

Fetai, B., Oštir, K., Fras, M., Lisec, A. (2019). Extraction of visible boundaries for cadastral mapping based on UAV imagery. *Remote Sens.*, 11(13), 1510. DOI: 10.3390/rs11131510.

Fetai, B., Račič, M., Tekavec, J. et al. (2020). Detection of visible boundaries from UAV images using U-Net. The International Archives of the Photogrammetry, Remote Sensing and Spatial Information Sciences, XLIII-B1-2020, 437–442.

François, C. et al. (2015). Keras. Retrieved from March 9, 2021, https://github.com/fchollet/keras.

Galarreta, J., Kerle, N., and Gerke, M. (2015). UAV-based urban structural damage assessment using object-based image analysis and semantic reasoning. *Nat. Hazards and Earth Syst. Sci.*, 15, 1087–1101. DOI: 10.5194/nhess-15-1087-2015.

Giuliani, D. (2012). Edge detection from MRI, DTI images with an anisotropic vector field flow using a divergence map. *Algorithms*, 5(4), 636–653. DOI: 10.3390/a5040636.

Gupta, R. (2016). *Enhanced edge detection technique for satellite images. International Conference on Cloud Computing and Security*. China: Springer, pp. 273–283.

Heipke, C., Mayer, H., Wiedemann, C.O. et al. (1997). Evaluation of automatic road extraction. *Int. Arch. Photogramm. Remote Sens.*, 47–56.

Horkaew, P., Puttinaovarat, S., and Khaimook, K. (2015). River boundary delineation from remote sensed imagery based on SVM and relaxation labelling of water index and DSM. *J. Theor. Appl. Inf. Technol.*, 71(3), 376–386.

Jazayeri, I., Rajabifard, A., and Kalantari, M. (2014). A geometric and semantic evaluation of 3D data sourcing methods for land and property information. *Land Use Policy*, 36, 219–230. DOI: 10.1016/j.landusepol.2013.08.004.

Jena, K.K., Mishra, S., and Mishra, S. (2015). Edge detection of satellite images: A comparative study. *Int. J. Innov. Sci., Eng. Tech.*, 2(3), 75–79.

Karabin, M., Bakula, K., and Luczynski, R. (2021). Verification of the geometrical representation of buildings in cadastre using UAV photogrammetry. *Geomat. Environ. Eng.*, 15(4), 81–99. DOI: 10.7494/geom.2021.15.4.81.

Kohli, D., Crommelinck, S., and Bennett, R. (2017). Object-based image analysis for cadastral mapping using satellite images. In Proceedings of the International Society for Optics and Photonics, Image Signal Processing Remote Sensing XXIII; SPIE. The International Society for Optical Engineering: Warsaw, Poland.

Kohli, D., Unger, E.-M., Lemmen, C. et al. (2018). Validation of a cadastral map created using satellite imagery and automated feature extraction techniques: A case of Nepal. In Proceedings of the FIG Congress, 6-11 May, pp. 17, Istanbul, Turkey.

Lakhani, K., Minocha, B., and Gugnani, N. (2016). Analyzing edge detection techniques for feature extraction in dental radiographs. *Perspectives in Science*, 8(4), 395–398. DOI: 10.1016/j.pisc.2016.04.087.

Luo, X., Bennett, R.M., Koeva, M. et al. (2017). Investigating semi-automated cadastral boundary extraction from airborne laser scanned data. *Land*, 6(3), 60. DOI: 10.3390/land6030060.

Manyoky, M., Theiler, P., Steudler, D. et al. (2011). Unmanned aerial vehicle in cadastral applications. International Archives of the Photogrammetry, Remote Sensing and Spatial Information Science, XXXVIII-1/(September), pp. 57–62. DOI: 10.5194/isprsarchives-XXXVIII-1-C2257-2011.

Martha, T.R., Kerle, N., van Westen et al. (2011). Segment optimization and data-driven thresholding for knowledge-based landslide detection by object-based image analysis. *IEEE Trans. Geosci. Remote Sens.*, 49(12), 4928–4943. DOI: 10.1109/TGRS.2011.2151866.

McGlone, J.C., and Shufelt, J.A. (1994). Projective and object space geometry for monocular building extraction. *IEEE Conf. Comput. Vis. Pattern Recogn.*, 54–61.

Munyati, C. (2018). Optimizing multiresolution segmentation: delineating savannah vegetation boundaries in the Kruger National Park, South Africa, using Sentinel 2 MSI imagery. *International J. Remote Sens.*, 39, 997–6019. DOI: 10.1080/01431161.2018.1508922.

Neubert, M., Herold, H., and Meinel, G., (2007). Assessing image segmentation quality – concepts, methods and application. *Lecture Notes in Geoinformation & Cartography*, 769–784. DOI: 10.1007/978-3-540-77058-9_42.

Nyandwi, E. (2018). The battle of cadastral intelligence: measuring the results of competition between people and machine in creation of cadastral boundaries. MSc thesis submitted to Enschede: University of Twente, Faculty of GeoInformation and Earth Observation (ITC). Retrieved from .

Pal, N.R., and Pal, S.K. (1993). A review on image segmentation techniques. *Pattern Recognition*, 26(9), 1277–1294. DOI: 10.1016/0031-3203(93)90135-J.

Parida, P.K., Sanabada, M.K., and Tripathi, S. (2014). Cadastral resurvey using high resolution satellite ortho image-challenges: A case study in Odisha, India. *Int. Arch. Photogram., Remote Sens. Spat. Inf. Sci.*, 40(8), 1165–1170. DOI: 10.5194/isprsarchives-XL-8-1165-2014.

Punarselvam, E., and Suresh, P. (2011). Edge detection of CT scan spine disc image using canny edge detection algorithm based on magnitude and edge length. In 3rd International Conference on Trendz in Information Sciences & Computing (TISC2011). Chennai, India, pp. 136–140.

Puniach, E., Bieda, A., Cwiakala, P., et al. (2018). Use of Unmanned Aerial Vehicles (UAVs) for Updating Farmland Cadastral Data in Areas Subject to Landslides. *ISPRS Int. J. Geoinf.*, 7(8):331. DOI: 10.3390/ijgi7080331.

Qui, K., Sun, K., Ding, K. et al. (2016). A fast and robust algorithm for road edges extraction from Lidar data. *Int. Arch. Photogram., Remote Sens. Spat. Inf. Sci.*, 693–698. DOI: 10.5194/isprs-archives-XLI-B5-693-2016.

Rijsdijk, M., van Hinsbergh, W.H.M., Witteveen, W. et al. (2013). Unmanned Aerial Systems in the process of Juridical verification of Cadastral border. *ISPRS Int. Arch. Photogramm. Remote Sens. Spat. Inf. Sci.*, XL-1/W2, 325–331. DOI: 10.5194/isprsarchives-XL-1-W2-325-2013.

Selvakumar, P., and Hariganesh, S. (2016). The performance analysis of edge detection algorithms for image processing. International Conference on Computing Technologies and Intelligent Data Engineering, 7-9 January Kovilpatti, India, pp. 1–5.

Sirmacek, B., and Unsalan, C. (2010). Road network extraction using edge detection and spatial voting. International Conference on Pattern Recognition, pp. 3117–3120. Istanbul, Turkey.

Taha, L.G.E., and Ibrahim, R.E. (2021). Assessment of Approaches for the Extraction of Building Footprints from Pléiades Images. *Geomat. Environ. Eng.*, 15(4), 101–116. DOI: 10.7494/geom.2021.15.4.101.

Wassie, Y.A. (2016). Toward automatic cadastral boundary mapping from satellite imagery. Thesis submitted to the Faculty of Geo-Information Science and Earth Observation of the University of Twente in partial fulfilment of the requirements for the degree of Master of Science in Geoinformation Science and Earth Observation.

Wassie, Y.A., Koeva, M.N., Bennett, R.M. et al. (2018). A procedure for semi-automated cadastral boundary feature extraction from high-resolution satellite imagery. *J. Spat. Sci.,* 63(1), 75–92. DOI: 10.1080/14498596.2017.1345667.

Witharana, C., and Civco, D.L. (2014). Optimizing multi-resolution segmentation scale using empirical methods: exploring the sensitivity of the supervised discrepancy measure Euclidean distance 2 (ED2). *ISPRS J. Photogram. Remote Sens.*, 87(1), 108–121. DOI: 10.1016/j.isprsjprs.2013.11.006.

Zevenbergen, J., and Bennett, R. (2015). The visible boundary: More than just a line between coordinates. In Proceedings of the GeoTech Rwanda, International Conference on Geospatial Technologies for Sustainable Urban and Rural Development, Kigali, Rwanda, 18-20 November, pp. 1–4.

Zhang, X., Xiao, P., Song, X. et al. (2013). Boundary-constrained multi-scale segmentation method for remote images. *ISPRS J. Photogram. Remote Sens.*, 78, 15–25. DOI: 10.1016/j.isprsjprs.2013.01.002.